

The Experimental Investigation of Corona Discharge Induced Wall Jet

Zhi-yan Chen

A thesis

submitted in partial fulfillment of the
requirements for the degree of

Master of Science

University of Washington

2019

Committee:

Igor Novosselov

Alberto Aliseda

Alexander Mamishev

Program Authorized to Offer Degree:

Mechanical Engineering

©Copyright 2019

Zhi-yan Chen

University of Washington

Abstract

The Experimental Investigation of Corona Discharge Induced Wall Jet

Zhi-yan Chen

Chair of the Supervisory Committee:

Igor Novosselov

Department of Mechanical Engineering

Corona discharge-induced wind is created when high-voltages applied across sharp electrodes and larger-radius ground electrode. This study examines the characteristics of the electrohydrodynamic wall jet driven by corona discharge in the surface boundary layer. The experimental setup includes a sawtooth electrode with peaks spaced 5mm apart, with distance from the tip to the ground varying from 9 to 18mm in 3mm increments. Voltage was then applied across the system from 5kV to 18kV in 1kV increments. Two corona regimes, glow and streaming discharge, generated the ionic wind. Experiments show spanwise and vertical similar velocity profiles for both regimes. The shallow cavity at the anode tip aids ionization, which results in a stable ionic wind generation. Velocity is correlated with electrical current in the system. The corona transitions from the glow to the streaming regime was observed when the conductance of the system was greater than 0.004mA/V. The efficiency in converting electrical energy to mechanical wind energy increases as the voltage is increased while in the glow regime, to a maximum of 2.5% at 10kV, 15mm electrode separation. Transitioning to streaming discharge the efficiency dropped due to rapid increase in current while only modest increase in momentum injection.

Acknowledgements

I would like to express my appreciation to Dr. Igor Novosselov for his support, suggestions, and direction during this research work. His willingness to give his time so generously has been very much appreciated.

Thank you also to the members of my committee, Dr. Alberto Aliseda and Dr. Alexander Mamishev for their time and evaluation of my work.

I would also like to thank my parents for all they have done.

Table of Contents

Abstract	iii
Acknowledgements.....	iv
Table of Contents	v
1. Introduction	1
2. Experiments	4
2.1. Description of Experimental Setup	4
2.2. Experimental Results.....	6
3. Energy Transfer Efficiency	18
4. Conclusion.....	20
Works Cited	22

1. Introduction

Electrohydrodynamic (EHD) flow, also referred as corona wind or ionic wind has been studied in multiple applications such as convective cooling¹⁻², electrostatic precipitators³⁻⁵, airflow control⁶, surface particle trapping⁷ and electroconvection⁸⁻⁹.

A high voltage applied to an electrode creates an electric field that ionizes gas particles^{10,11}. This electric field region is referred to as the corona. In a positive corona, negatively charged species return to the anode, and positive ions drift towards the cathode¹². The ions collide and transfer momentum to neutral gas molecules, and the bulk movement of the gas molecules generates this movement. The corona generation is reliant on high voltage coupled with low current. While higher current may generate a more visible corona, there is also a higher chance of arcing between the electrodes, which collapse the corona. Five regions of discharge have been observed, dependent on the electric field strength¹³ and researchers have explored their stability as a function of the electric current, finding the most stable being in the generalized glow region with current on the order of 0.5mA/m^2 ¹⁴⁻¹⁵. At such conditions, a maximum velocity of 5m/s can be induced by the corona. Zhakin¹⁰ found the electric field strengths on the order of 10^3 kV/cm to generate these coronas, resulting in voltage sources between 5kV and 50kV for typical ionic wind propulsion experimental setups¹⁶⁻¹⁸. A solid-state propulsion plane flown by Xu et al¹⁹ used a 40kV power source to fly, with a wingspan of 5m, obtaining 2.5% conversion from electrical to mechanical wind power. A quadratic relationship between the voltage and current characteristics and a linear relationship between the voltage and wind velocity are described in the literature, e.g.¹⁰.

Optimization studies found that a positive electrode to a ground or a positive electrode to a negative electrode generates a stronger electric field than a negative electrode to ground²⁰.

Furthermore, stable voltage and induced DC current are preferable to AC current. There is a threshold voltage where the electric field is generated and ionization starts, prior to this there is no ionization. This threshold voltage is reduced for sharp points or thin wires geometries²¹.

Furthermore, various corona configurations, such as a wire to rod¹⁴, point to ring²², point to plate²³, wire to plate²⁴, or coaxial cylinders²⁵ have been explored for the generation of the corona. The investigation into point to ring corona discharge combined with a numerical simulation by Guan et al.²² found efficiency on the order of 1% can be achieved, with a velocity of 5m/s at 7mm electrode separation. The maximum velocity of 9m/s can be achieved with an electrode separation of 3mm. The efficiency at that point is decreased due to a less parallel electric field between the electrodes. The corona discharge can be used as a fluid pump with no moving parts²⁶, but the efficiency is also low, ~ 0.8%²⁷.

A surface corona discharge near the wall can be used to modify the airflow in the boundary layer, drag reduction, and separation control on airfoils at higher angles of attack²⁸. Touchard and Moreau²⁹ studied the effects of corona discharge on NACA 0015 airfoils, observing boundary layer separation at 15° angle of attack. An induced flow of 0.4m/s is sufficient to cause the reattachment of the boundary layer for a flat plate. Ketcham et al.³⁰ have studied the effect of corona discharge on the laminar to turbulent transition point on a flat plate. The transition point shifted by 43mm for an external free stream velocity of 53 m/s.

Several researchers have studied drag reduction using corona discharge on a flat plate³¹⁻³². Moreau and Léger³³ observed reductions at a maximum velocity of 2.75 m/s for 500 μ A current with an external free stream. A drag reduction of 30% was observed. Other experiments find drag reductions on the order of 20% for low Reynolds-Number external flow with EHD³⁴⁻³⁵.

A major limitation of these setups is the upper limit of voltage that is imposed by the generation of filamentary streamers and arcing between the electrodes. The presence of streaming or arcing acts as a short between the electrodes, reducing or eliminating the voltage difference between them and thus the field³⁶. A dielectric barrier physically separating the electrodes to reduce, creating dielectric barrier discharge, has been observed to have promising results, allowing for higher voltages to be used before breakdown³⁷. They are also less sensitive to ambient humidity³⁸. The efficiency of such is on the order of 0.1% electrical to mechanical energy³⁹. This is well below the efficiency values found in literature for corona discharge.

In this thesis, a planar corona discharge in the wall boundary layer on a flat plate is investigated. The flow is studied experimentally to resolve the spatiotemporal characteristics of the velocity field. The electrical to kinetic energy transfer efficiency is calculated for the experiments, and the influencing factors of the electric field to are investigated.

2. Experiments

2.1. Description of Experimental Setup

The EHD flow is studied on a conducting flat plate with a shallow rectangular cavity. Figure 1 shows the schematic representation of corona discharge induced flow in the wall boundary layer region on a conducting flat plate with a cavity. Its objective is to accelerate the flow near the wall to modify the boundary layer profile. The serrated edge copper electrode with a thickness of 0.2mm serves as the anode. The pitch of the sawtooth is 5mm. The ground electrode is a 1.5mm thick steel rod. The flat plate is fabricated using 3D printing in the polylactic acid polymer. A shallow rectangular cavity of 15 mm wide and 1.3 mm deep is built into the flat plate to aid ionization. The anode overhangs the backward-facing step of the cavity by 3mm, as shown in Figure 2 such that the distance between the anode tips and cathode (L) is 9mm. The width of the experimental setup is 100 mm. The cathode is flush mounted against the forward-facing step, see Figure 1. The top of the electrode protrudes 0.2mm above the flat plate. The cathode protrusion results in the Stokes flow, not affecting the downstream velocity profile development.

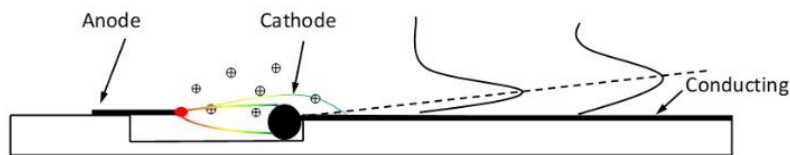


Figure 1: Schematic diagram of the corona driven EHD wall jet; colored lines show electrical field line, solid lines the down – velocity profile.

A variable high-voltage DC power supply (Bertan 205B-20R) is used to set the electrical potential between the electrodes. The cathode current is measured based on the voltage drop across

a $1\text{M}\Omega$ resistor. The distance between the tip of the anemometer probe and the center of the cathode rod (D) is varied.

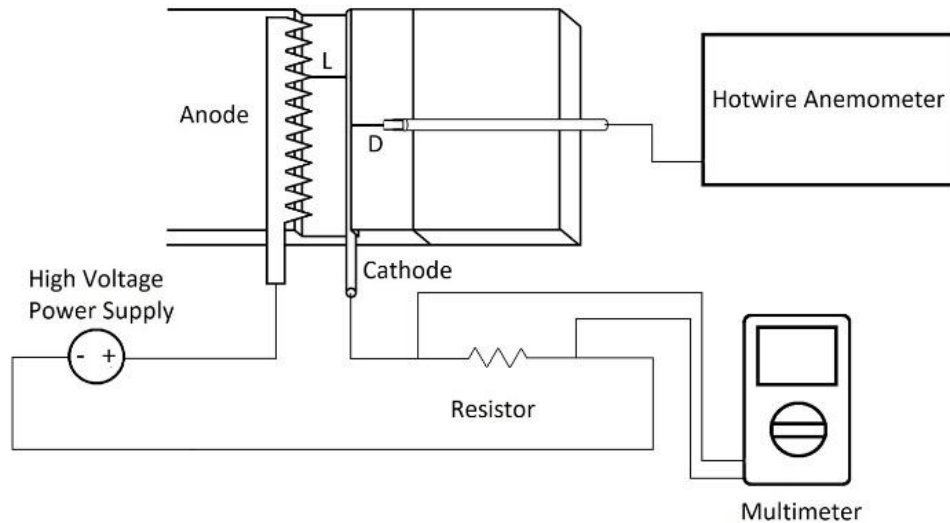


Figure 2: Schematic of the experimental setup. A DC high voltage is applied between the copper sawtooth anode and a steel rod cathode, the distance between the anode and cathode is determined by the 3D printed base plate the electrodes are attached to.

The anemometer was calibrated for a range of velocities 0.2 - 5m/s. Calibration was performed by setting up an external flow pump connected to a 1m long pipe. A dry flow meter was connected between the pipe and the pump. The air velocity was then calculated by dividing the volumetric flow by the cross-section of the pipe. The hot-wire anemometer voltage for a velocity range of 0.2m/s to 5m/s in approximately 20 steps were measured. The flow in the pipe transitions from laminar flow to turbulent flow over the velocity sweep complicates the analysis, the voltage values for the transition zone velocities were interpolated from values for laminar and purely turbulent regions. The data were collected at a frequency of 20kHz using a data acquisition module (myRIO-1900, National Instruments Inc.), with a sampling time of 30 seconds. The anemometer probe was mounted on an optical 3D stage; movement is controlled by

micrometers with a range of 40mm. The anemometer probe holder is 1mm in diameter, but 300mm long. Due to the weight of the probe holder, the probe is presented tilted at a slight angle to the plate. The anemometer readings are blind to the direction of flow except for reverse flow, so the readings are not affected.

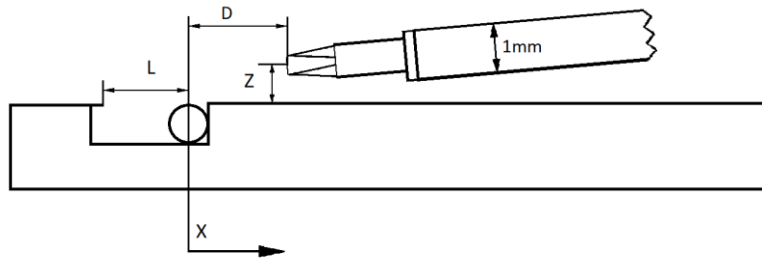


Figure 3: A side view of the anemometer, the ground, and the sawtooth. The anemometer tip is a thin wire across the two prongs. Measurements are made from the center of the wire to the center of the ground rod. The distance L is varied by changing the setup, other values are changed by moving the anemometer probe.

2.2. Experimental Results

2.2.1 Current – Voltage Relationship

In the initial experiments, the sawtooth anode was set to 9mm from the cathode on the 3D printed plate. The anemometer probe was not used for these experiments. The power supply was turned on, and the voltage was incremented in steps of 1kV until an anode current from the power supply was detected. This value is considered the corona inception voltage as described by Loeb¹², and the voltage was incremented in steps of 1kV every 5 minutes. The time interval between the measurement allows the current and voltage to stabilize. At 11kV, the electrode began to spark and indicates the voltage limit for the 9mm configuration. The configuration was modified by increasing the distance between the anode and the cathode to 12mm, then 18mm.

For the 12mm configuration, the voltage sweep resulted in current from 8kV to 12kV, and for the 18mm, from 14kV to 18kV. The current-voltage relationship was noted by measuring the current created per voltage, at each voltage setting. The relationship is plotted in Figure. 4. The cathode current is between 70-85% of the anode current, indicating ion charges accumulating on the apparatus, 15-30% of ions flow is not recovered by the cathode.

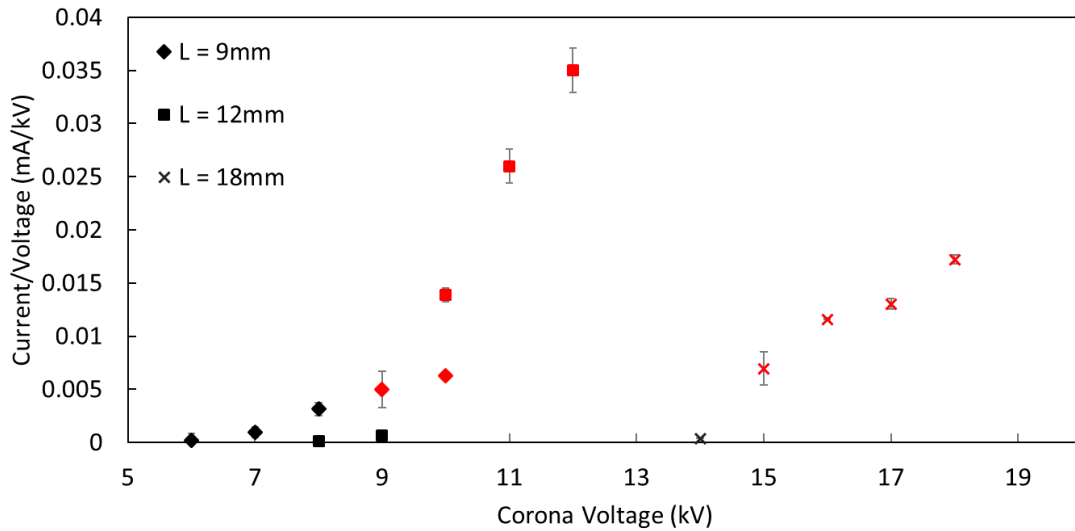


Figure 4: The current-voltage measurements. The data in red shows the regions where the streamers in the corona discharge are visible.

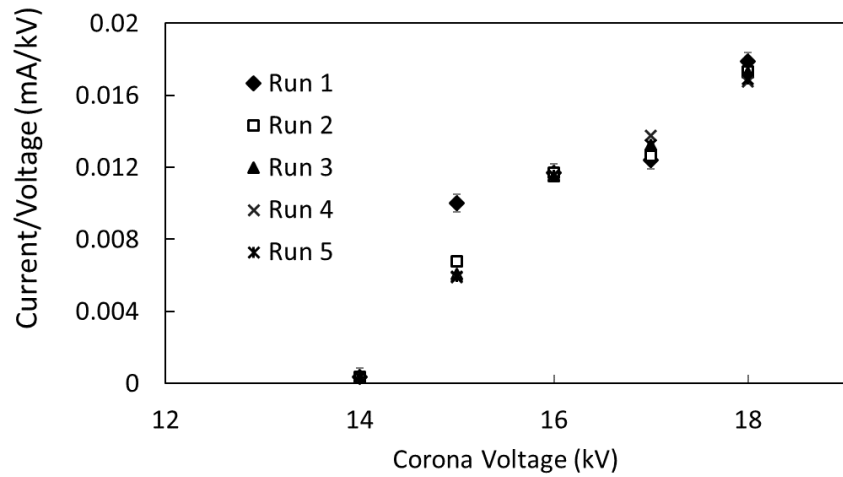
The current for L=9mm at 6kV is 0.0015mA, corresponding to a current density of 0.015mA/m. The current then increases as the voltage is increased, up to 0.07mA at 10kV, before the spark-over occurs. Changes in the corona regimes can be observed as the voltage increases. At lower voltage, two regimes can be observed: (i) where there is a measurable current, but no wind is measured, for the L=9mm case, this is observed at 6kV. (ii) At the 7kV and 8kV voltages, but below a 0.005mA/kV threshold, the corona displays characteristics of the glow regime described by Leger et al. ⁶ In this regime, there is a measurable velocity generated,

and a small glow along the tips of the electrode can be observed. The voltage at the low end of where the glow regime starts is corona inception voltage, in this case, 7kV.

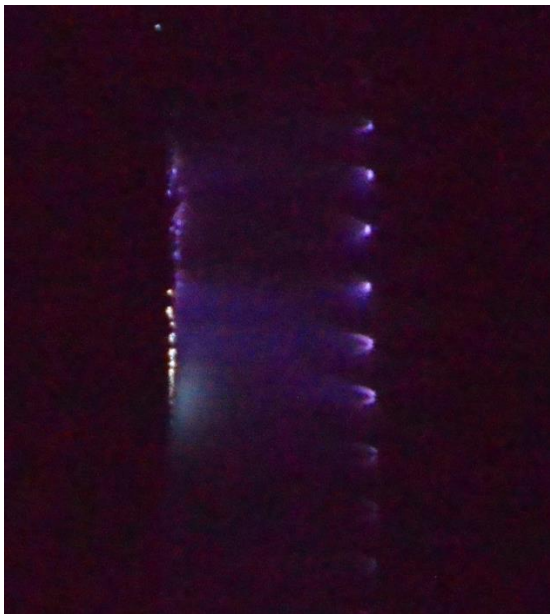
As the voltage is increased to 9kV, the conductance is greater than 0.005mA/kV threshold, and the corona discharge enters the streaming regime, also described by Leger et. Al. The most obvious physical characteristic is a noisy crackle that is generated by the corona. Furthermore, the corona glow becomes a sheet of discharge between the electrodes, resulting in the entire space between the electrodes to glow. There is a measurable velocity in this discharge regime.

Increasing the voltage past 11kV results in the breakdown of the corona and into the spark-over regime, where a conductive pathway from the anode to the ground is momentarily created by the electron discharge. There is no wind generation once the corona breaks down.

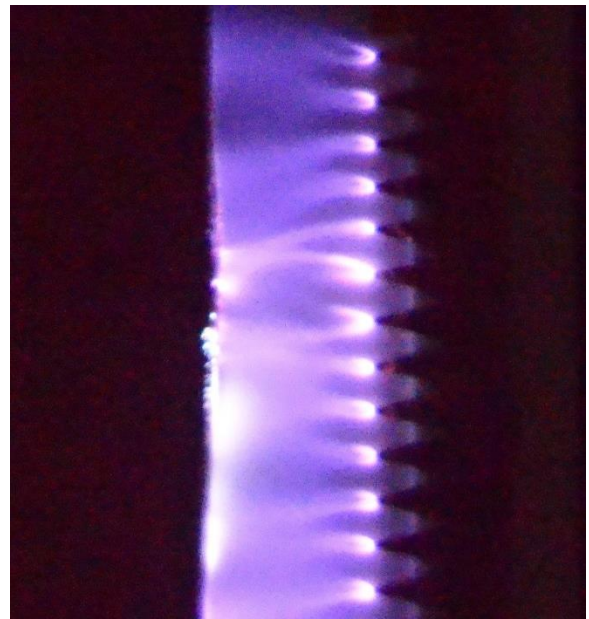
A similar progression occurs for other geometries. For all set-ups, the glow to streaming occurs near 0.005mA/kV, indicating that it is dependent on the conductance, however, the transition from streaming to arcing does not have a common threshold. Since corona inception voltage is also a property of the setup geometry¹², but independent of conductance, it is possible for the corona inception voltage to initialize with a conductance beyond 0.005mA/kV. This happens in the L=18mm condition, where there is no measurable glow regime. Specifically, as seen in figure 5, the corona inception voltage at 15kV already results in a conductance above 0.005mA/kV.



a)



b)

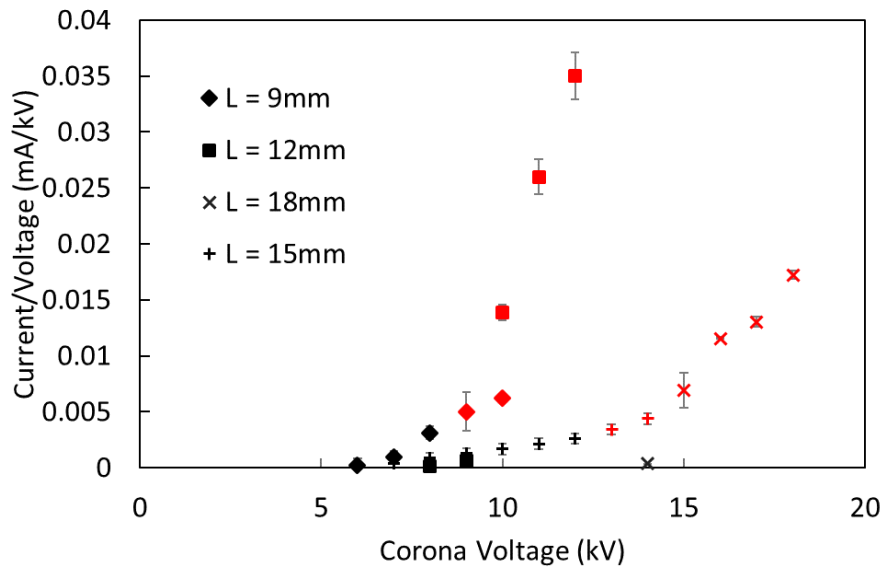


c)

Figure 5. Corona behavior for at 18mm electrode separation. a) The current per voltage increases with voltage. There was no run where the corona inception voltage initiated within the glow regime. b) The streaming discharge at 15kV, at the low end of the streaming regime. c) The discharge at 18kV. The streaming is quite noticeable from the tips of the sawtooth to the ground.

2.2.1.1 Corona discharge of the 15mm plate

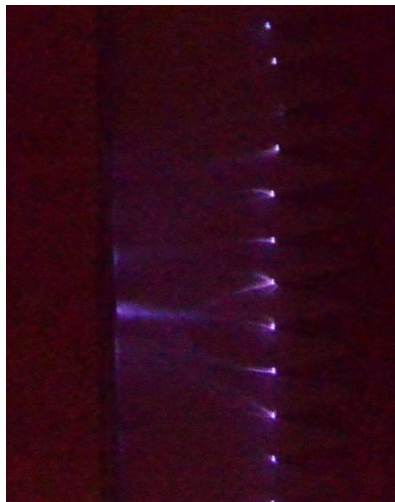
The 15mm plate was utilized to further explore the voltage-current relationship. The experiments here were done with a separate setup. The results are displayed in figure 7.



a)



b)



c)



d)

Figure 7. The results of further investigation of the 15mm plate in a separate location. a) The results of the voltage sweep from the CIV of 6kV to arcing beyond 14kV, compared to the results of the previous experiment. b) The physical appearance of the glow regime. The corona appears circular at the tip of the sawtooth. c) The streaming regime. In comparison with the 18mm streaming regime, the individual filaments are more visible at the lower velocity. d) An arcing event between the electrodes. An arcing event is not sustained compared to the streaming and is significantly more visible and audible.

In this case, the conductivity threshold appears to have decreased from 0.005mA/kV to 0.004mA/kV, as a result of the current jump from glow to streaming not being as large as expected. Furthermore, the corona inception began at 6kV, significantly less than expected, given that the 12mm CIV was 7kV. The arcing voltage is also below expectations. These factors suggest the 15mm setup, created and experimented separately from the rest of the setups, have lower resistance to current flow. It should be noted however that the 15mm 10kV point, denoted in green in figure 7, was taken with the original setup.

The conductance threshold should also be revisited, as the 0.005mA/kV value was where the streaming begins to appear for the original set of experiments, but the conductance jump from glow to streaming along with the 1kV voltage increments limit the resolution of the experiments around the transition zone.

2.2.2 Velocity – Voltage Relationship

The second set of experiments is aimed to characterize the airflow that is generated by the corona. Specific voltages for investigation were determined from the current-voltage experiments. The criteria for selection was a stable corona and current. The anemometer probe is placed at the appropriate distance away from the ground in the x-axis (10mm), and the micrometer reading is noted. The micrometer base is set to the midpoint of its range, and the anemometer is placed at the mid-point in the spanwise location. The anemometer probe is then

moved to the spanwise initial position along the y-axis with the fine adjustment, starting directly opposite a sawtooth tip, and the micrometer reading noted. Finally, the probe is lowered to the initial position above the plate in the z-axis, and the reading noted again. The data collection is initiated, and the voltage is set to the experimental value.

After the initial 5 minutes, to allow the system to achieve steady-state, the anemometer reading is taken, and the probe advanced in the Y-direction in 2.5mm intervals. The measurements are taken every 1 minute at each probe relocation. The procedure is repeated for a total span of 30mm to generate one y-sweep for each x and z value.

The probe is then reset to the starting position on the y-axis, and the z-axis location is adjusted by 1 mm. The y-sweep is then run again. The range of the experiments for the z-axis is from 1mm to 6mm. The anemometer base is moved via micrometer 10mm away from the previous X position and the sweeps are run again.

2.2.2.1 Spanwise Velocity Profile

From the spanwise measurements, the effect of the sawtooth can be clearly seen, see Figure 9. Vaddi et al's experiments with ionic wind suggest ionic wind generation from points act like a jet⁵, and experiments done by Wilson et al. describe the generation of wind across the plate as a wall jet.²⁰ The wall jet is generated at the tip of the sawtooth, so the distance to the anemometer increases with the electrode separation distance. The effect of streamline vortex formation on development of flow structures is possible, however, the flow visualization was not performed in this study.

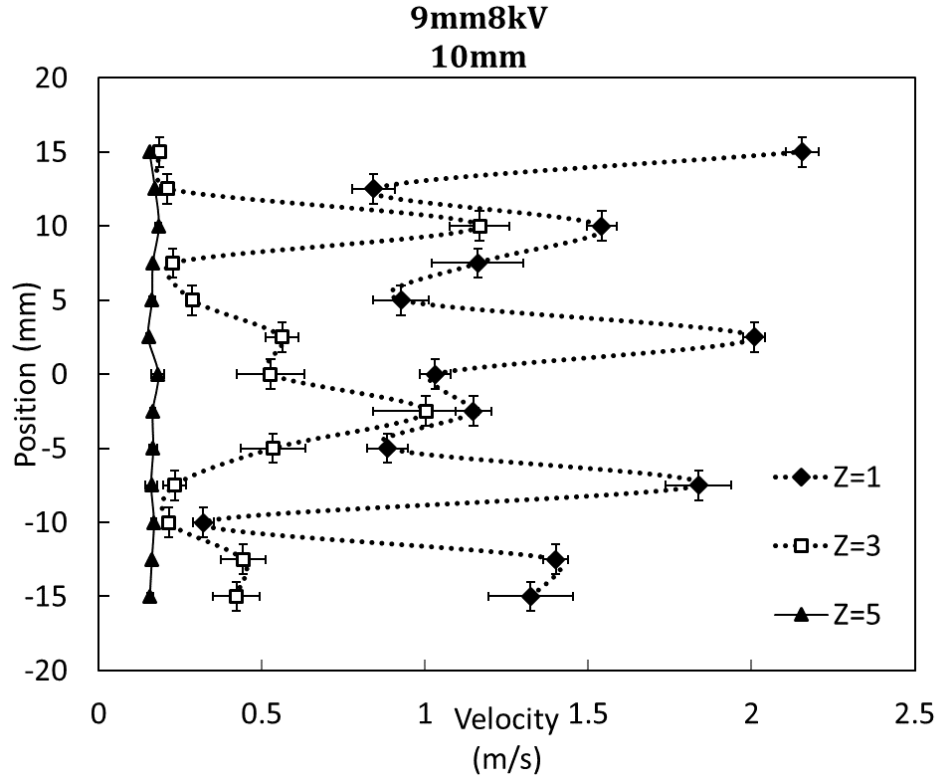


Figure 8: The spanwise sweep for the 9mm electrode separation setup. The profiles for $Z=2$ and 4 were omitted for clarity, but the effect of the sawtooth can be clearly seen on the velocity, as well as the rapid decay in velocity above the plate.

2.2.2.2 Wall Jet Profile

In order to increase the applied voltage without entering the streaming regime, the distance between the electrodes is increased. The increase in voltage offsets the decrease in current that accompanies the increases in separation distance, resulting in a net increase in energy input and thus wall jet momentum. The increase in wall jet momentum injection can be observed in Figure 10. The maximum velocities are similar likely due to the similarity in the momentum dissipation in the viscous boundary layer independent of distance between the cathode and anode. The analysis of wall similarities may shed further insight into this behavior⁴⁰.

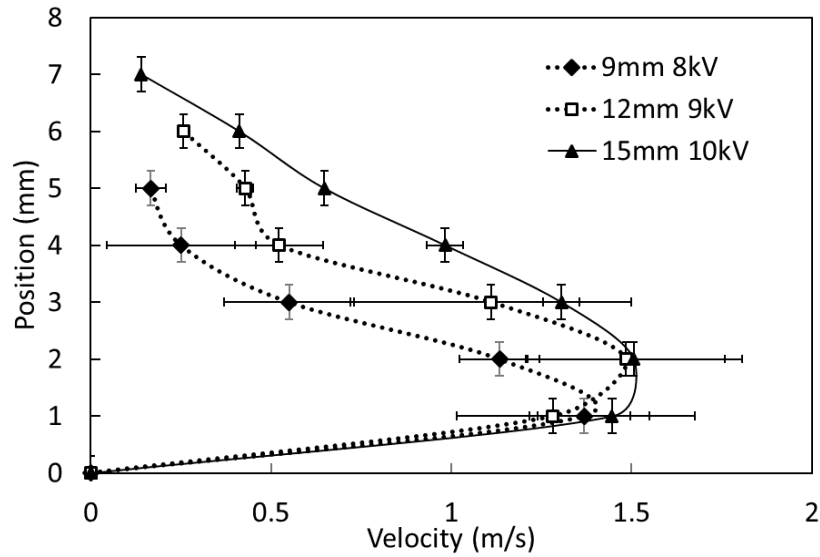


Figure 9. The average velocity profiles of the glow discharge-induced flow. The maximum velocity does not appear to increase but the increased entrainment as the distance from the sawtooth tip is increased is clear.

This increased distance to the sawtooth allows us to observe the development of the wall jet as the flow develops along the X-axis, such as in Figure 10. Figure 9 shows that the individual jets are defined with high peak velocities and low valley velocities. However, as the distance from the sawtooth electrode increase, the jets expand and the velocity range decrease. Vortices and jet-jet interaction play a role in reducing flow profile non-uniformity in spanwise direction. Figure 11 shows the jet development of the jet for the 12mm non-streaming condition. There is no airflow detected at $Z=5\text{mm}$ above the surface at 10mm from the ground. However, downstream, the jet has clearly expanded due to momentum displacement associated with the wall jets. At the highest distance from the jet point (Figure 12), the individual jets from the tips of the sawtooth are no longer visible as the jet merging⁴³ is observed.

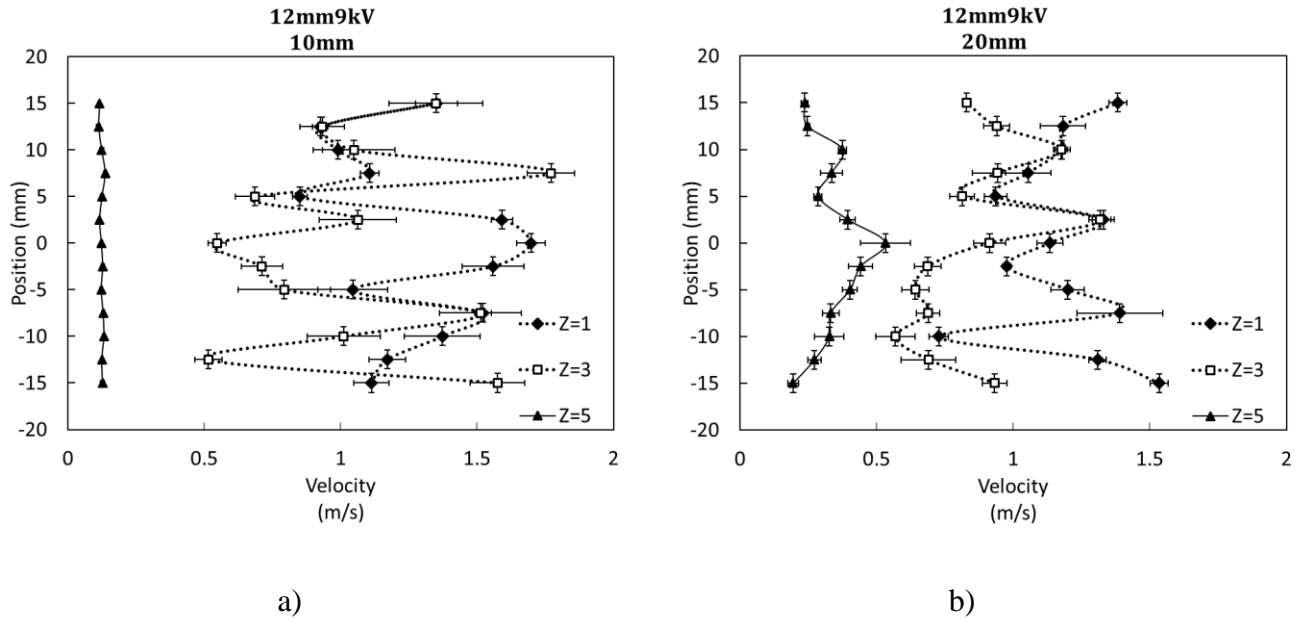


Figure 10. The spanwise velocity profiles of the sawtooth corona-induced wall jet. a) the individual sawtooth location can still be seen although the jet flow has already expanded, and the jet entrainment smoothens the profile. b) the individual jets have expanded and are in the process of combining.

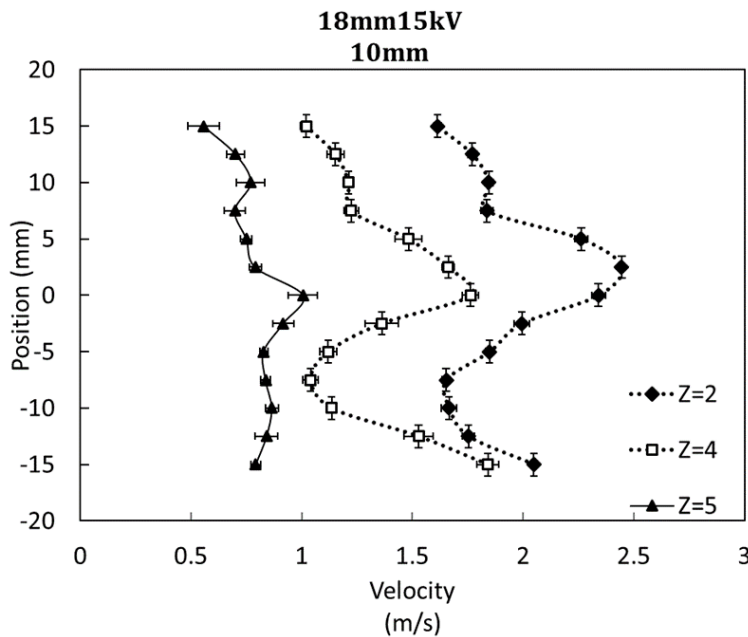


Figure 11. Spanwise wall jet pattern as a function of z coordinate.

2.2.3 Discussion of Streaming Regime

The increase in voltage is associated with an increase in energy input, which correspondingly increases the velocity. However, at the transition between the glow and streaming discharge, maximum velocity does not increase. As seen in Figure 12, for the case of 12mm, there is little change in both the maximum velocity and the spanwise velocity profile as the voltage is increased from 9kV to 10kV. The overall momentum, however, increases slightly due to a greater thickness of the wall jet. This increase in voltage also resulted in an increase in current, from 23 μ A to 32 μ A.

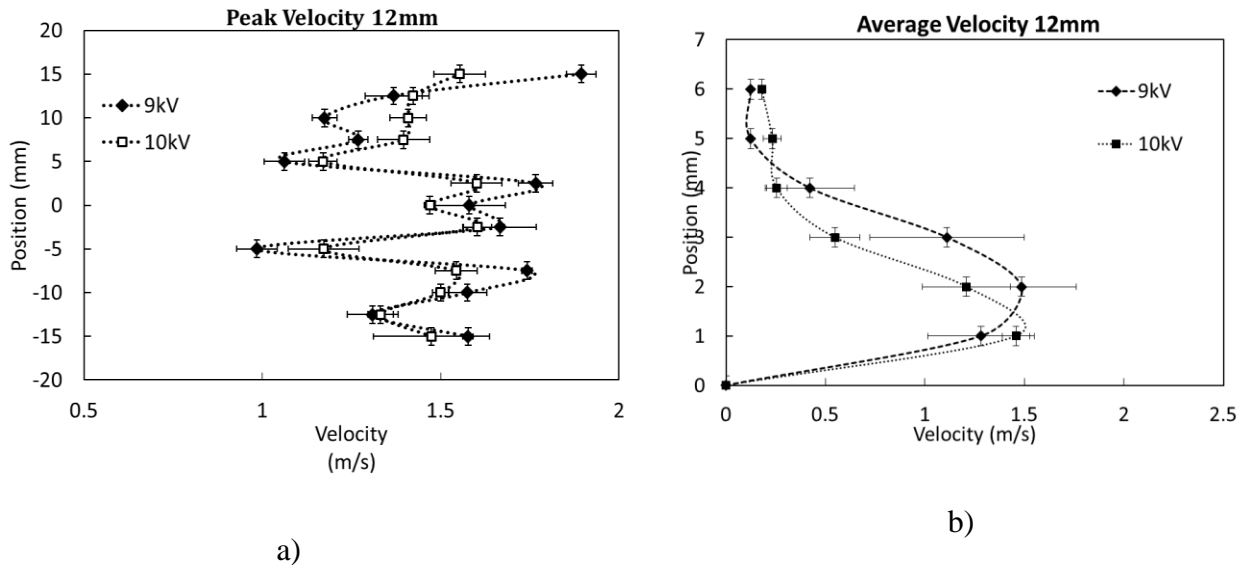


Figure 12. a) The spanwise flow profile of the 12mm setup at peak velocity, measured 10mm from the ground. b) The voltage increase does not meaningfully change the horizontal profile. The vertical velocity growth has been reduced, however.

The increase in voltage and energy in streaming regime does not result in the same momentum increase as in the glow regime. As seen in Figure 13, the velocity profile for the 18mm setup does not change with increased voltage. The current, however, increases significantly, from 180 to 370 μ A. This indicates the increase in energy from both the voltage

and current does not increase the velocity. The wall jet velocity profile for the 17kV case does not decay smoothly. This is thus evidence of larger 3D eddies present in the flow that were not there at lower voltages. The generation of these 3D eddies may indicate flow generation from locations other than at the tips of the sawtooth, as the concentration of charge on the electrode reaches saturation at the tips and spread through the rest of the electrode.

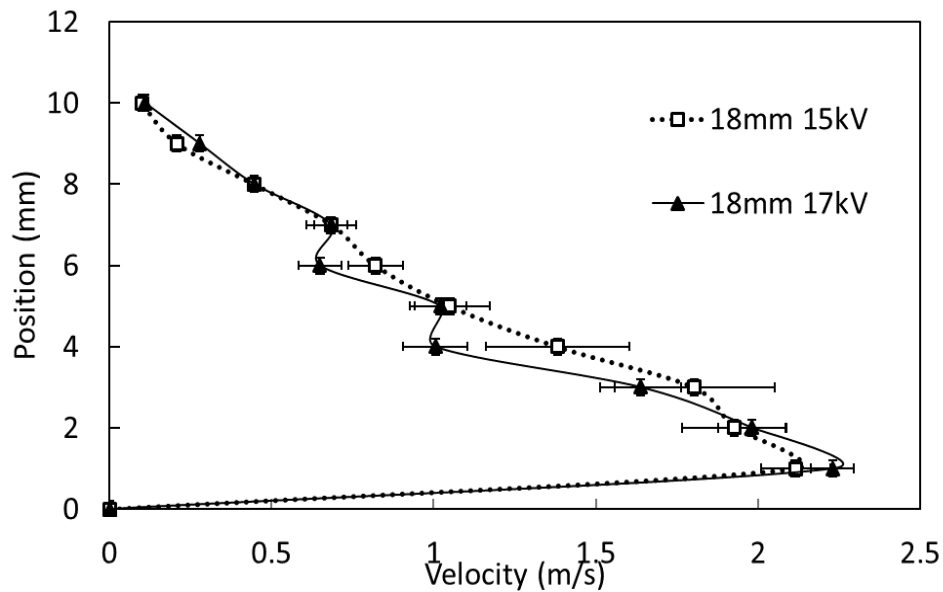


Figure 13. The velocity profile of the 18mm experiments. The increase in energy from 15kV to 17kV appears to have no effect on maximum velocity or increased entrainment, but the effect can still be seen as the decay of velocity from the plate shows evidence of larger flow structures.

The wall jet development as a function of glow vs streaming discharge in the wall boundary layer needs to be further investigated. The study is complicated by the inconsistencies in the wall jet profiles with environmental conditions.

3. Energy Transfer Efficiency

The application of corona discharge in either thrust generation or airflow control is dependent on the efficiency of the system in converting electrical power into mechanical power. This can be computed by estimating the ratio of the kinetic energy of the flow to the electrical power provided by the power source:

$$\eta = \frac{\left(\frac{1}{2}\right)\rho \int u^3 dA}{\phi I}$$

The resulting efficiency is presented in Tables 1 and 2, separated by the discharge regime.

Table 1. Glow Corona Efficiency.

	8kV 9mm	9kV 12mm	10kV 15mm
Efficiency (%)	2.0 ± .4	2.0 ± .4	2.5 ± .4
Anode Current (μA)	35	23	20
Kinetic Energy (W)	0.0057	0.0042	0.0053

Table 2. Streaming Corona Efficiency.

	9kV 9mm	10kV 12mm	15kV 18mm	17kV 18mm
Efficiency (%) ± 20%	2.4	1.11	0.71	0.32
Anode Current (μA)	45	32	180	370
Kinetic Energy (W)	0.0099	0.0035	0.0190	0.0175

The maximum efficiency can be observed at the highest voltage applied before the streaming transition, as the increased voltage is offset by the decrease in current caused by increasing the distance between the two electrodes. Past the streaming transition, decreasing the current in this way does not yield efficiency gains as the velocity of the wind is significantly reduced. In general, the streaming corona is less efficient than the glow corona in energy conversion.

For 9mm cases, the highest efficiency is observed at the transition from glow to streaming regimes. The efficiency within the streaming zone decreases as more electrical energy is pushed through the system. This efficiency loss can be observed physically as the streamers become more audible as the voltage is increased, along with velocity measurements done in experiment 2 that show the slower boundary layer growth in the streaming regimes.

Despite the low efficiency, however, the most kinetic energy obtained was in the streaming zone, with the 18mm, 15kV case. Although more electrical energy can be pumped into the system, the flow velocity does not rise.

4. Conclusion

Two sets of experiments were performed in order to characterize the corona-induced wall jet from a sawtooth electrode. In the first set of experiments, the corona discharge characteristics were examined. Measurements of the current for applied voltages between 5 to 18kV were taken for experimental setups with electrode separations of 9mm, 12mm, 15mm and 18mm. From these measurements, it was found both the current and the rate of increase in current, or conductance, increase as the applied voltage increases. The shallow cavity at the anode tip aids ionization, which results in a stable corona discharge.

The system exhibits 4 regions as the electrical field increases. At lower voltages, the corona is inconsistent due to the partial corona onset, not all tips are energized. As voltage increases, the corona develops at the tips of the sawtooth electrode, creating the glow regime. As voltage increases, causing the current to increase beyond the 0.004mA/V threshold, the corona transitions to the streaming regime, covering the area between the electrodes with a sheet of purple. Beyond this streaming discharge, the corona breaks down and electrical arcing between the electrodes start. The threshold is dependent on the setup and the experimental conditions, as further experiments are needed to characterize the threshold.

The second set of experiments investigated the velocity profiles of the discharge. Horizontal velocity profiles show that the flow is highest opposite the tips of the sawtooth. The maximum velocities are about 2.5 m/s. Vertical velocity profiles are characteristic of wall jet profiles. In the vertical case, the peak velocity, and thus the boundary layer growth, has been shifted closer to the flat plate when the corona is streaming.

In the glow regime, increasing the voltage increases the electrical to mechanical energy, with a maximum efficiency in these experiments of 2.5%. Within the streaming regime, the

highest efficiency, at 2.4%, was observed at the transition from glow to streaming. As the current increases within the streaming regime, the efficiency decreases.

Works Cited

- [1] L. Zhao, K. Adamiak and M. Mazumder, "Numerical and Experimental Studies of the Electrohydrodynamic Pump for Sampling System on Mars," 2008.
- [2] T. Yokoyama, M. Kogoma, T. Moriwaki and S. Okazaki, "The mechanism of the stabilisation of glow plasma at atmospheric pressure," *Journal of Physics D: Applied Physics*, vol. 23, no. 8, pp. 1125-1128, 1990.
- [3] L. Y. Yeo, D. Hou, S. Maheshwari and H. C. Chang, "Electrohydrodynamic surface microvortices for mixing and particle trapping," *Applied Physics Letters*, vol. 88, no. 23, 5 6 2006.
- [4] T. Y. Wen, T. T. Shen, H. C. Wang and A. Mamishev, "Optimization of wire-rod electrostatic fluid accelerators," in *Proceedings - Electronic Components and Technology Conference*, 2013.
- [5] R. S. Vaddi, Y. Guan and I. Novosselov, "Particle Dynamics in Corona Induced Electrohydrodynamic Flow".
- [6] H. Tsubone, J. Ueno, B. Komeili, S. Minami, G. D. Harvel, K. Urashima, C. Y. Ching and J. S. Chang, "Flow characteristics of dc wire-non-parallel plate electrohydrodynamic gas pumps," *Journal of Electrostatics*, vol. 66, no. 1-2, pp. 115-121, 1 2008.
- [7] F. Soetomo, "The influence of high voltage discharge on flat plate drag at low Reynolds number air flow The influence of high voltage discharge on flat plate drag at low Reynolds number air flow ⁴ / 99-2".
- [8] F. Soetomo, G. M. Colver and K. Forouraghi, "Micro-force measurement of drag on a small flat plate in the presence of a corona discharge," *Journal of Electrostatics*, vol. 64, no. 7-9, pp. 525-530, 7 2006.
- [9] H. Schlichting and K. Gersten, *Boundary-Layer Theory*, 9th ed., Verlag Berlin Heidelberg : Springer, Berlin, Heidelberg, 2017, p. 805.
- [10] J. R. Roth, "Aerodynamic flow acceleration using paraelectric and peristaltic electrohydrodynamic effects of a One Atmosphere Uniform Glow Discharge Plasma," *Physics of Plasmas*, vol. 10, no. 5, pp. 2117-2126, 25 4 2003.
- [11] M. Rickard, D. Dunn-Rankin, F. Weinberg and F. Carleton, "Maximizing ion-driven gas flows," *Journal of Electrostatics*, vol. 64, no. 6, pp. 368-376, 6 2006.

- [12] E. Moreau, R. Sosa and G. Artana, "Electric wind produced by surface plasma actuators: A new dielectric barrier discharge based on a three-electrode geometry," *Journal of Physics D: Applied Physics*, vol. 41, no. 11, 7 6 2008.
- [13] E. Moreau, L. Leger and G. Touchard, "Effect of a DC surface-corona discharge on a flat plate boundary layer for air flow velocity up to 25 m/s," *Journal of Electrostatics*, vol. 64, no. 3-4, pp. 215-225, 2006.
- [14] E. Moreau, C. Louste and G. Touchard, "Electric wind induced by sliding discharge in air at atmospheric pressure," *Journal of Electrostatics*, 2008.
- [15] N. Monrolin, F. Plouraboué and O. Praud, "Electrohydrodynamic Thrust for In-Atmosphere Propulsion," *AIAA Journal*, vol. 55, no. 12, pp. 4296-4305, 12 2017.
- [16] M. MALIK, L. WEINSTEIN and M. HUSSAINI, "Ion wind drag reduction," 2013.
- [17] P. Magnier, D. Hong, A. Leroy-Chesneau, J. M. Pouvesle and J. Hureau, "A DC corona discharge on a flat plate to induce air movement," *Journal of Electrostatics*, 2007.
- [18] L. B. Loeb, *Electrical coronas, their basic physical mechanisms*, Berkeley: University of California Press, 1965.
- [19] L. Léger, E. Moreau and G. G. Touchard, "Effect of a DC corona electrical discharge on the airflow along a flat plate," *IEEE Transactions on Industry Applications*, vol. 38, no. 6, pp. 1478-1485, 11 2002.
- [20] L. Leger, E. Moreau and G. Touchard, "Control of low velocity airflow along a flat plate with a DC electrical discharge," 2002.
- [21] K. J. Laidler, J. H. Meiser and B. C. Sanctuary, *Physical Chemistry*, Houghton Mifflin, 2002.
- [22] E. E. Kunhardt, L. H. Luessen and N. A. T. O. S. A. Division, *Electrical Breakdown and Discharges in Gases, Part B: Macroscopic Processes and Discharges*, NATO Scientific Affairs Division [by] Plenum Press, 1983.
- [23] I. A. Krichtafovitch, V. L. Gorobets, S. V. Karpov and A. V. Mamishev, "Electrostatic Fluid Accelerator and Air Purifier-The Second Wind".
- [24] D. B. Go, S. V. Garimella, T. S. Fisher and R. K. Mongia, "Ionic winds for locally enhanced cooling," *Journal of Applied Physics*, vol. 102, no. 5, 2007.

- [25] D. B. Go, R. A. Maturana, T. S. Fisher and S. V. Garimella, "Enhancement of external forced convection by ionic wind," *International Journal of Heat and Mass Transfer*, vol. 51, no. 25-26, pp. 6047-6053, 12 2008.
- [26] M. Forte, J. Jolibois, E. Moreau, G. Touchard and M. Cazalens, "Optimization of a Dielectric Barrier Discharge Actuator by Stationary and Non-stationary Measurements of the Induced Flow Velocity - Application to Airflow Control," in *3rd AIAA Flow Control Conference*, American Institute of Aeronautics and Astronautics, 2006.
- [27] S. El-Khabiry and G. M. Colver, "Drag reduction by dc corona discharge along an electrically conductive flat plate for small Reynolds number flow," *Physics of Fluids*, vol. 9, no. 3, pp. 587-599, 1997.
- [28] D. S. Drew, N. O. Lambert, C. B. Schindler and K. S. Pister, "Toward Controlled Flight of the Ionocraft: A Flying Microrobot Using Electrohydrodynamic Thrust with Onboard Sensing and No Moving Parts," *IEEE Robotics and Automation Letters*, vol. 3, no. 4, pp. 2807-2813, 1 10 2018.
- [29] E. A. CHRISTENSON and P. S. MOLLER, "Ion-neutral propulsion in atmospheric media.," *AIAA Journal*, vol. 5, no. 10, pp. 1768-1773, 1 10 1967.
- [30] D. BUSHNELL, "Turbulent drag reduction for external flows," in *21st Aerospace Sciences Meeting*, American Institute of Aeronautics and Astronautics, 1983.
- [31] G. Artana, J. D' Adamo, L. Léger, E. Moreau, G. Touchard, "Flow Control with Electrohydrodynamic Actuators," *AIAA Journal*, vol. 40, no. 9, pp. 1773-1779, 9 2002.
- [32] K. Adamiak and P. Atten, "Simulation of corona discharge in point-plane configuration," *Journal of Electrostatics*, vol. 61, no. 2, pp. 85-98, 6 2004.
- [33] "Major de Seversky's Ion propelled craft," *Popular Mechanics*, 8 1964.
- [34] Y. Guan and I. Novosselov, "Two Relaxation Time Lattice Boltzmann Method Coupled to Fast Fourier Transform Poisson Solver: Application to Electroconvective Flow," *arXiv preprint arXiv: 1812.05711*, 2018.
- [35] Y. Guan and I. Novosselov, "Numerical Analysis of Electroconvection Phenomena in Cross-flow," *arXiv preprint arXiv:1812.10899*, 2018.
- [36] A. Zhakin, "Electrohydrodynamics," *Physics - Uspekhi*, vol. 5, no. 55, pp. 465-488, 2012.
- [37] J. Wilson, H. D. Perkins and W. k. Thompson, "An Investigation of Ionic Wind Propulsion," NASA/TM, Cleveland, 2009.

- [38] E. Moreau, "Airflow control by non-thermal plasma actuators," *Journal of Physics D; Applied Physics*, vol. 40, pp. 605-636, 2007.
- [39] Y. Guan, R. S. Vaddi, A. Aliseda and I. Novosselov, "Experimental and numerical investigation of electro-hydrodynamic flow in a point-to-ring corona discharge," *Physical Review Fluids*, vol. 3, no. 4, 2018.
- [40] P. Fillingham, Y. Guan, R. S. Vadi and I. Novosselov, "Numerical, Experimental and Analytical Investigation of the Planar Electrohydrodynamic Wall jet," in *Bulletin of the American Physical Society*, Seattle, 2019.
- [41] J. KETCHAM and H. R. VELKOFF, "Effect of an electrostatic field on boundary- layer transition.," *AIAA Journal*, vol. 6, no. 7, pp. 1381-1383, 1 7 1968.
- [42] S. Marzouk Khairallah and N. Hnaien, "Numerical Study of Interaction of Two Plane Parallel Jets," *International Journal of Engineering, Transactions A: Basics*, vol. 29, pp. 1421-1430, 2016.